Shock and Vibration 19 (2012) 585–596
DOI 10.3233/SAV-2011-0652
IOS Press



# Improvement of accuracy in damage localization using frequency slice wavelet transform

Xinglong Liu[a,b,*], Zhongwei Jiang[b] and Zhonghong Yan[c]
[a]*National Engineering Laboratory for System Integration of High Speed Train (south), CSR Qingdao Sifang Co. Ltd, Qingdao, China*
[b]*Department of Mechanical Engineering, Engineering Faculty, Yamaguchi University, Ube, Japan*
[c]*Biomedical Department, Chongqing University of Technology, Chongqing, China*

Received 21 July 2011
Revised 13 September 2011

**Abstract.** Damage localization is a primary objective of damage identification. This paper presents damage localization in beam structure using impact-induced Lamb wave and Frequency Slice Wavelet Transform (FSWT). FSWT is a new time-frequency analysis method and has the adaptive resolution feature. The time-frequency resolution is a vital factor affecting the accuracy of damage localization. In FSWT there is a unique parameter controlling the time-frequency resolution. To improve the accuracy of damage localization, a generalized criterion is proposed to determine the parameter value for achieving a suitable time-frequency resolution. For damage localization, the group velocity dispersion curve (GVDC) of $A_0$ Lamb waves in beam is first accurately estimated using FSWT, and then the arrival times of reflection wave from the crack for some individual frequency components are determined. An average operation on the calculated propagation distance is then performed to further improve the accuracy of damage localization.

Keywords: Lamb wave, time-frequency analysis, frequency slice wavelet transform, dispersion curve, damage localization

## 1. Introduction

Structural safety is a topic of great significance in many fields, such as aerospace, civil infrastructure and some mechanical engineering structures. In order to ensure the structure safety and reliability, many non-destructive evaluation (NDE) techniques and structural health monitoring (SHM) techniques have been developed over several past decades. One primary objective of these techniques is to detect and localize damage in structure. Among them, elastic wave propagation especially Lamb waves are effectively used for this objective. The significant advantage using Lamb waves for damage detection and localization is that Lamb waves can travel a long distance with little attenuation, as well as have very high sensitivity to various structural defects [1–6].

The use of Lamb waves is complicated by the existence of multiple modes at any given frequency. Moreover, all the Lamb waves modes generally are dispersive, That is to say, the propagation velocity is dependent on the excitation frequency, which causes the shape of the propagating wave changes with distance along the propagation path. For this reason, generally a narrowband excitation signal is carefully designed to generate a specified Lamb waves mode which is less dispersive and also able to interact with small defects. This process is accomplished along with the consideration of numerous factors including the material properties and dimension of the structure to be

*Corresponding author. Tel.: +86 532 68953556; Fax: +86 532 87953551; E-mail: xinglong-liu@hotmail.com.

ISSN 1070-9622/12/$27.50 

interrogated, the size of type of transducers and the type of damage to be detected, etc [3,4,7–9]. Alternatively, a simple and easily manipulated method to generate Lamb waves is the impact excitation. When using this method, a broadband response will be induced. In consequence, the exact arrival time or time of flight (TOF) is difficult to determine. Recently time-frequency analysis is popularly used in the analysis of dispersive Lamb waves. Such analysis allows the isolation of individual frequency component of Lamb waves and thus permits the localization of damage more effectively.

Short Time Fourier Transform (STFT), Winger-Ville distribution (WVD) and Continuous Wavelet Transform (CWT) are most commonly used in the characterization of time-varying spectral components of signals. However, STFT and WVD have some limitations in time-frequency analysis in comparison with CWT. Due to the fixed time-frequency resolution achieved in STFT, STFT is inappropriate for the analysis of a wave signal whose instantaneous frequency varies rapidly [10]. WVD has excellent time-frequency resolution, but the cross-term is introduced into WVD, which causes spurious artifacts and may lead to misinterpretation of the signal phenomenon. The cross-term can be smoothed out, but will reduce the resolution in return. In contrast to STFT and WVD, CWT possesses the property that the bandwidth to the center-frequency ratio is constant, i.e., the window function of CWT automatically narrows for detecting high frequency component and widens for investigating low frequency component. Owning to the advantageous feature, CWT can more accurately extract the instantaneous frequency information of the signal.

Recently Yan et al. [11] developed a new method for time-frequency analysis called as frequency slice wavelet transform (FSWT). This method has the similarly essential feature of adaptive resolution like CWT, and ncludes some new useful features. The detailed description of this method is discussed in the published paper [11].

In this paper, FSWT is introduced to perform time-frequency analysis of Lamb waves signal for damage localization. The simple and practical impact excitation is used to generate Lamb waves, and the surface-bonded PZT sensor is used to receive Lamb waves. In the first section of the paper, the fundamental of FSWT is briefly stated. Due to the important effect of time-frequency resolution on the accuracy of damage localization, an approach is proposed to achieve optimal time-frequency resolution. In the scenario of damage localization, FSWT-based time-frequency analysis is first used to extract the GVDC of $A_0$ Lamb waves from impact-induced Lamb waves signal. After damage is induced in the beam, the arrival time of reflection wave from the crack is determined based on FSWT-based time-frequency analysis. Using the information of group velocity and arrival time, the crack is therefore localized.

## 2. Fundamental of frequency slice wavelet transform

The fundamental of FSWT is briefly given here. The FSWT of a signal $f(t) \in L^2(R)$ is defined as [11]

$$W(\omega, t) = \frac{1}{2\pi} \int_{-\infty}^{+\infty} \hat{f}(u) \hat{p} * \left( \frac{u-\omega}{\sigma} \right) e^{iut} du \tag{1}$$

where asterisk denotes the complex conjugate, $\hat{f}(u)$ is the Fourier transform of $f(t)$ and $\hat{p}(u)$ is the frequency slice function (FSF) in frequency domain, which is similar to the wavelet basis of CWT, $\sigma$ is the scale parameter in frequency domain. In general, it is reasonably assumed that the parameter $\sigma$ is proportional to the analyzing frequency $\omega$, and is taken as $\sigma = \frac{\omega}{\kappa}$. The FSWT is then expressed as

$$W(\omega, t) = \frac{1}{2\pi} \int_{-\infty}^{+\infty} \hat{f}(u) \hat{p} * \left( \kappa \frac{u-\omega}{\omega} \right) e^{iut} du \tag{2}$$

In Eq. (2), the time-frequency window is adaptive to the observing center frequency of the analyzed signal, and the scale $\kappa$ is a balance factor between the time resolution and the frequency resolution. With this definition, the window width of FSF $\hat{p}$ is narrow at low frequencies and becomes wide at high frequencies. Thus, FSWT has the similar feature of adaptive resolution as CWT. However, for FSWT the reconstruction condition is $\hat{p}(0) \neq 0$ or $\hat{p}(0) = 1$. It is obvious that this condition is weaker than the admissibility condition of CWT, and hence can be satisfied more easily. There are many filters can be used as the FSF, such as

$$\text{(I) } \hat{p}(\omega) = e^{-\frac{1}{2}\omega^2}; \text{ (II) } \hat{p}(\omega) = \begin{cases} 1 & |\omega| \leqslant \omega_0 \\ 0 & |\omega| > \omega_0 \end{cases}; \text{ (III) } \hat{p}(\omega) = \frac{\sin \omega}{\omega}; \text{ (IV) } \hat{p}(\omega) = \frac{1}{1+|\omega|^n}.$$

The inverse FSWT to reconstruct the original signal is expressed as

$$f(t) = \frac{1}{2\pi} \int_{-\infty}^{+\infty} W(\omega, \tau)\, e^{i\omega(t-\tau)} d\tau d\omega \tag{3}$$

Due to the weak reconstruction condition for FSF, the parameter value of $\kappa$ that controls the time-frequency resolution can be determined over a wide range to meet the requirement of time frequency analysis. However, in CWT, the wavelet basis necessarily satisfies the strict admissible condition, which restricts the effective use of CWT for time-frequency analysis. For instance, in the most commonly used Morlet wavelet, the admissibility condition limits the selection of the constant bandwidth to center-frequency ratio, which is a vital parameter affecting the accuracy of time-frequency analysis [10,12]. Furthermore, an inconvenience existed in CWT is that the scale partition number in the frequency axis should be considered prudently, because it is also an important factor related with the accuracy of time frequency analysis [6,13], and the scale value must be converted to frequency value for physical interpretation. In contrast to CWT, such consideration and operation are not needed in the implementation of FSWT. It is also noticed that the reconstruction Eq. (3) is also quite different from CWT in that the inverse transform of FSWT is not directly related with the FSF $\hat{p}$. Moreover, Eqs (1)–(3) can be efficiently computed with aid of Fast Fourier Transform (FFT) algorithm.

## 3. Determination of suitable time-frequency resolution in FSWT

In the implementation of FSWT, the first step is to design a suitable FSF. The FSF can be freely designed to meet the need of signal analysis under condition $\hat{p}(0) = 1$. Since the Gaussian function has the smallest Heisenberg resolution in time-frequency plane, it is chosen as FSF

$$\hat{p}(\omega) = e^{-\frac{\omega^2}{2}} \tag{4}$$

Once the FSF has been selected, the parameter to be determined is only the scale factor $\kappa$ in Eq. (2).

As discussed above, the parameter $\kappa$ controls the variation of window width of $\hat{p}$ with frequency and hence directly determines the frequency resolution. Because of Heisenberg uncertainty principle it also simultaneously affects the time resolution. The time-frequency resolution significantly influences the accuracy of damage localization in the time-frequency analysis of Lamb waves signal. For achieving a reasonable compromise between time and frequency resolution, Yan et al. [11,14] discussed the determination of $\kappa$ based on the characteristics of the analyzed signal. However, the characteristics of the analyzed signal are generally not known *a priori*, and it is strongly signal-dependent. With the aim of improving the accuracy of damage localization, a generalized criterion is proposed to determine the optimal parameter value.

The concept of Shannon entropy comes from the field of information theory. It measures the degree of uncertainty in a system [15]. It is also a measure of energy concentration and has been used in the selection of wavelet basis [6, 16]. For a one-dimensional of time series $S = \{s_i\}_{1 \leqslant i \leqslant N}$, Shannon entropy function is defined as

$$H_1(S) = -\sum_i p_i \log p_i \tag{5}$$

where

$$p_i = \frac{|s_i|^2}{\|S\|^2}, \sum_{i=1}^{N} p_i = 1 \text{ and } \|S\|^2 = \sum_{i=1}^{N} |s_i|^2.$$

By the definition of $H_1(S)$, it is bounded by $0 \leqslant H_1(S) < \log N$. The Shannon entropy function shown above is a measure of energy concentration, the higher the signal energy concentration is, the lower the entropy cost is. For instance, if $p_i$ are zero for all except $p_k = 1$, the entropy value $H_1(S)$ becomes zero. If all $p_i$ are the same value, i.e. $1/N$. the entropy value is equal to $\log N$.

In the evaluation of Shannon entropy for the two-dimensional time-frequency coefficient $W(t, \omega)$, the discrete form of $W(t, \omega)$ is given as

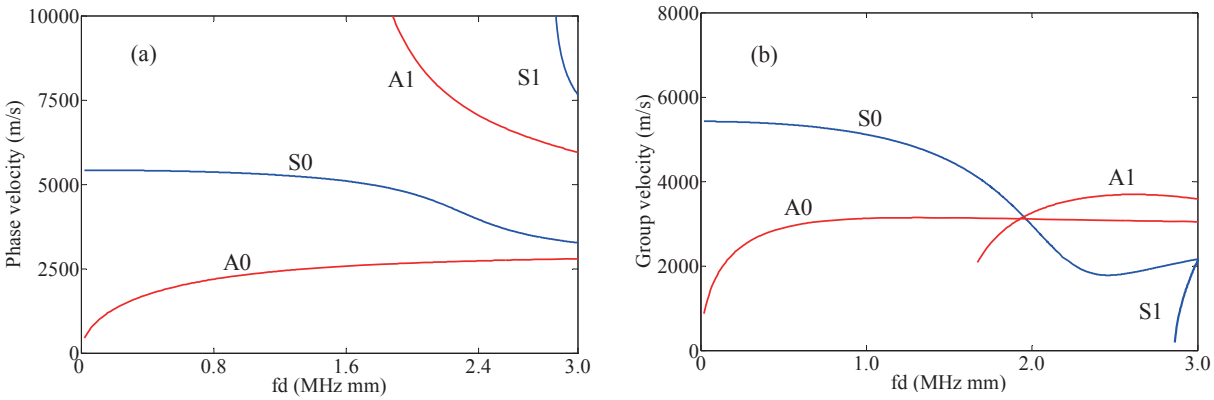


Fig. 1. Dispersion curves for Lamb waves in an aluminum plate: (a) phase velocity and (b) group velocity.

$$w_{i,j} = W(\omega_i, t_j) \quad (i = 1, ..., m) \text{ and } (j = 1, ..., n) \tag{6}$$

The two-dimensional Shannon entropy function for $w_{i,j}$ is defined as

$$H_2(W) = \sum_i \sum_j \frac{w_{i,j}^2}{|W_i|^2} \log\left(\frac{w_{i,j}^2}{|W_i|^2}\right) \tag{7}$$

where

$$|W_i|^2 = \sum_{j=1}^{n} |w_{i,j}|^2$$

is the square norm of coefficients $w_{i,j}$ for each frequency value $\omega_i$. The optimal value $\kappa_{opt}$ that maximizes the time-frequency energy localization can be determined by minimizing the entropy of equation

$$\kappa_{opt} = \arg\min_{\kappa} H_2(W). \tag{8}$$

## 4. Application of FSWT in Lamb wave-based damage detection

### *4.1. Estimation of the GVDC of $A_0$ Lamb wave in beam*

Lamb waves are guided waves that propagate through plate-like structure [17]. There are two types of Lamb waves: symmetric mode (S mode) and antisymmetric mode (A mode). In practical applications of Lamb waves, $S_0$ mode and $A_0$ are usually used for damage detection. The dispersion curves for Lamb waves in an aluminum plate are plotted in Fig. 1. It is seen that below 0.8 MHz mm frequency-thickness product $A_0$ mode has much shorter wavelength and lower velocity compared with $S_0$ mode. Therefore, $A_0$ mode is more sensitive to some minor damages and has better time resolution. Nevertheless, within such frequency domain, $A_0$ mode is more dispersive than $S_0$ mode does.

The behavior of $A_0$ Lamb waves in beam structures can be described by Bernoulli-Euler theory and Timoshenko theory [18]. Since Bernoulli-Euler theory assumes that the cross-section of the beam remains plane and normal to the neutral axis during bending, it is only applicable for $A_0$ Lamb waves propagation in thin beam at low frequencies. In contrast, Timoshenko beam formulation accounts for the shear deformation and rotational inertia effects. Thus, it is able to accurately describe the behavior of $A_0$ Lamb waves in relatively thick beam over wide frequency range. The phase velocity of $A_0$ Lamb waves calculated by Timoshenko theory is given as [19]

$$c_p = c_0 \left[\frac{(1+\alpha)\bar{\omega}^2 - \sqrt{(1+\alpha)^2\bar{\omega}^4 - 4\alpha\bar{\omega}^2(\bar{\omega}^2 - 12\alpha)}}{2(\bar{\omega}^2 - 12\alpha)}\right]^{1/2} \tag{9}$$

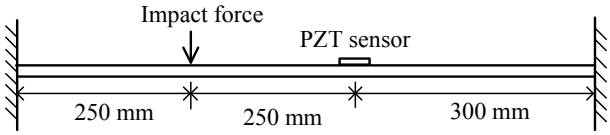


Fig. 2. A fixed-fixed beam bonded with PZT sensor subjected to impact.

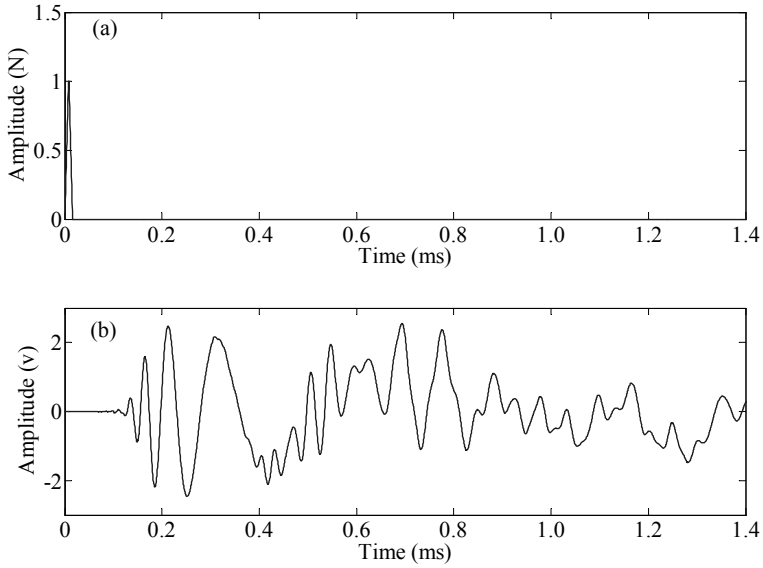


Fig. 3. Time response signal of (a) impact force and (b) the acquired $A_0$ Lamb wave.

where

$$c_0 = \sqrt{\frac{E}{\rho}}, \alpha = \frac{\gamma}{2\,(1+v)}, \bar{\omega} = \frac{h}{c_0}\omega,$$

$h$ is the thickness of the beam, $E$ is the Young's modulus of the beam, $v$ is Poisson's ratio, $\rho$ is the material density and $\gamma$ is the shear coefficient. The group velocity defined as $\bar{c}_g = d\bar{\omega}/d\bar{k}$ is yielded as [19]

$$\bar{c}_g = \frac{(1+\alpha)\,\bar{\omega}^2 - 2\alpha\bar{k}^2}{2\bar{\omega}^2 - (1+\alpha)\,\bar{k}^2 - 12\alpha}\,\frac{1}{c_p} \tag{10}$$

Equations (8)–(9) show that the phase and group velocity vary with frequency, implying the dispersive nature of Lamb waves.

The GVDC of Lamb waves are the primarily crucial information for damage localization. Therefore, FSWT-based time-frequency analysis is first performed to estimate the GVDC of $A_0$ Lamb waves in beam. FEM package ANSYS was first utilized to generate the simulated Lamb waves signal. Figure 2 shows the schematic configuration of an aluminum beam bonded with PZT sensor. The sizes of the beam is 800 mm × 20 mm × 3 mm. The PZT sensor with sizes of 15 mm × 10 mm × 0.3 mm is bonded onto the beam surface at 500 mm from the left end of the beam. The impact force is applied perpendicularly to the beam surface at 250 mm from left end of the beam. The time history of the impact force is a triangle impulse, of which time response linearly rises to constant peak value of 1 N at 0.016 ms and then linearly falls zero at 0.032 ms (see Fig. 3a). The impact force normal to the beam surface mainly generates the transverse wave motion in the beam. As a result, the signal with large, low frequency $A_0$ mode is produced. Although the smaller amplitude $S_0$ mode is produced simultaneously, it will not affect the detection and analysis of $A_0$ Lamb waves signal. In ANSYS, three-dimensional element type of solid 185 is used to discretize the fixed-fixed beam, and piezoelectric element type of solid 5 is used to discretize the PZT sensor. The mass matrix

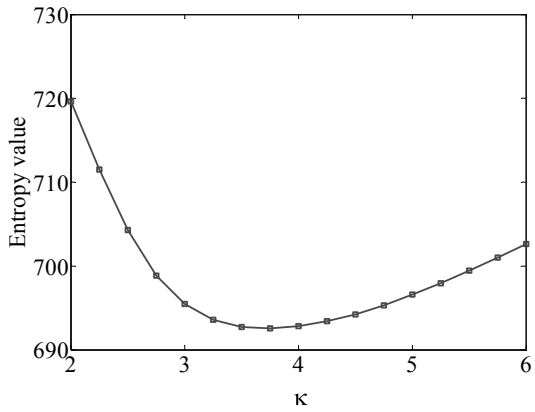


Fig. 4. Entropy value versus $\kappa$ for the time-frequency plane of the simulated signal.

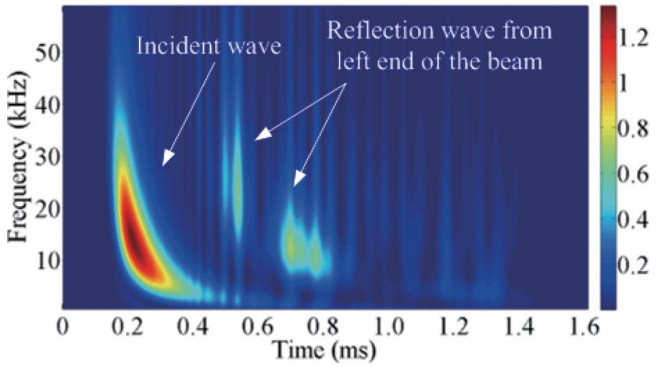


Fig. 5. Time-frequency distribution plane with $\kappa = 2.0$.

multiplier for damping $\alpha = 2000$ is specified in the FE model [20]. To obtain accurate high frequency wave signal, the element length is set at 1 mm and the time step size is $5 \times 10^{-4}$ ms. The material density of aluminum beam is 2700 kg/m$^3$, the Young's modulus is 70 GPa and the Poisson's ratio is 0.345.

The signal acquired from the PZT sensor is shown in Fig. 3b. To estimate the GVDC of $A_0$ Lamb waves using the acquired signal with FSWT, Shannon entropy function is used to choose a suitable time-frequency resolution in FSWT. The procedure for achieving the optimal value of $\kappa$ is explained as follow: First a range of values of $\kappa$ and a constant interval are given respectively, some discrete values of $\kappa$ are then determined. For each value of $\kappa$, the time-frequency coefficients resulted from FSWT of the signal is obtained, then the corresponding entropy of the time-frequency coefficients is calculated using Eqs (6)–(7). Based on Eq. (8), the minimum entropy value of all the entropy values represents the optimal value of $\kappa$. Using this procedure, the variation of entropy value versus $\kappa$ is shown in Fig. 4 and the optimal value of $\kappa$ is $\kappa_{opt} = 3.75$. To verify the effectiveness of the proposed criteria, the time-frequency distribution plane with a given value $\kappa = 2.0$ is displayed in Fig. 5. Note that the time-frequency distribution plane is the square magnitude of FSWT, which is corresponding to the spectrogram of STFT or scalogram of CWT. In Fig. 5 it is apparent that the frequency resolution after 0.4 ms begins to drop and the reflection wave from the left end of the beam is distorted. As a result, the arrival time of the reflection wave extracted from such time-frequency plane is inevitably quite inaccurate. While for the optimal value $\kappa_{opt} = 3.75$, the time-frequency distribution plane is shown in Fig. 6. A good compromise between time resolution and frequency resolution is achieved in the time-frequency plane.

The time-frequency plane of Fig. 6 is used to estimate the GVDC of $A_0$ Lamb waves mode. The distance between the impact position and the sensor position is $d = 250$ mm. The start time of incident wave at all the frequencies is known as $t_i\,(f) = 0.016$ ms, which is the peak value of the triangular impulse. The arrival time of the incident wave at each frequency, propagating from impact position to the sensor position, is defined as $t_a\,(f)$. For a given frequency

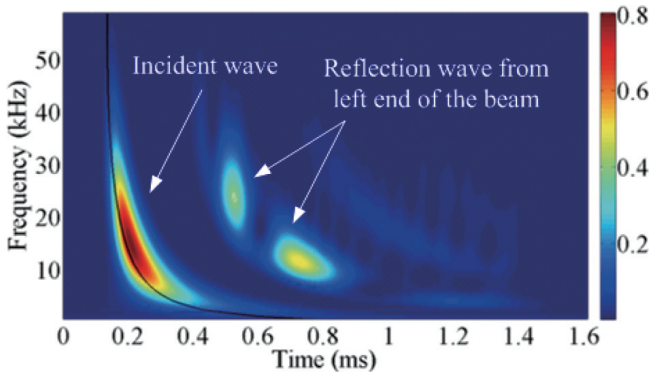


Fig. 6. Time-frequency distribution plane with $\kappa_{opt} = 3.75$.

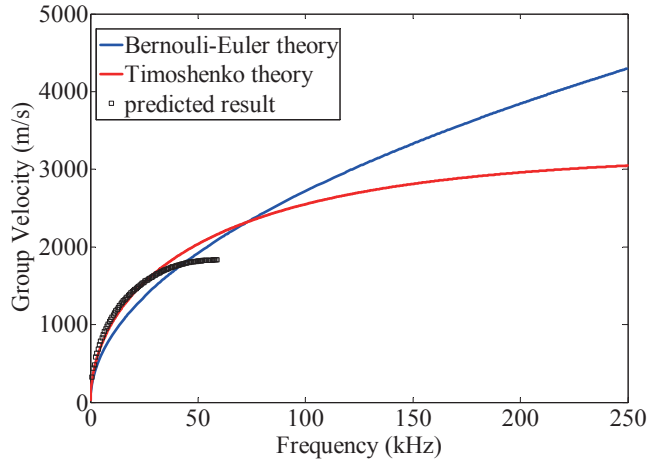


Fig. 7. The GVDC of A0 Lamb wave in beam estimated from simulation signal.

represented on the vertical axis of the time-frequency plane in Fig. 6, the first-arrived local peak indicates the arrival time of the frequency component wave. In this way, the arrival time over wide frequency range is identified and plotted with a black line in Fig. 6. The TOF value is defined as $\Delta t\,(f) = t_a\,(f) - t_i\,(f)$. Therefore, the group velocity at each frequency is expressed as

$$c_g\,(f) = \frac{d}{\Delta t\,(f)} = \frac{d}{t_a\,(f) - t_i\,(f)} \tag{11}$$

With aid of FSWT-based time-frequency analysis, the group velocity estimated is plotted with open circle in Fig. 7. The theoretical GVDC calculated by Timoshenko theory as well as Bernouli-Euler theory is also plotted in Fig. 7. It is seen that the estimated dispersion curve agrees better with Timoshenko theory than Bernouli-Euler beam theory. This result demonstrates that the time-frequency resolution selected based on the proposed criterion of the Shannon entropy is effective to determine accurate arrival time of dispersive wave.

### *4.2. Experimental verification for the GVDC estimated with using FSWT*

A schematic illustration of the experimental setup is shown in Fig. 8. A 30 mm wide and 3 mm thick aluminum beam specimen under fixed-fixed boundary condition is used. One PZT patch (PZT C-6, Fuji Ceramics Corporation) of 3 mm $\times$ 3 mm $\times$ 0.3 mm as sensor is bonded onto the end of the fixed-fixed beam specimen, which is served as the trigger for the whole data acquisition process. Another PZT patch of 7 mm $\times$ 5 mm $\times$ 0.3 mm is also bonded onto the beam surface. The time response data acquired from this PZT sensor is used to estimate the GVDC and

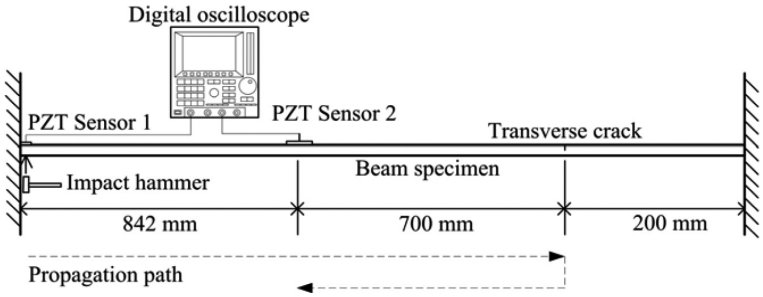


Fig. 8. A schematic illustration of the experimental set-up.

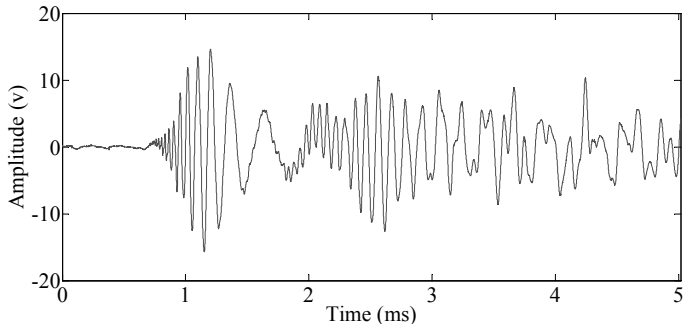


Fig. 9. Time response signal measured from sensor 2 at pristine state.

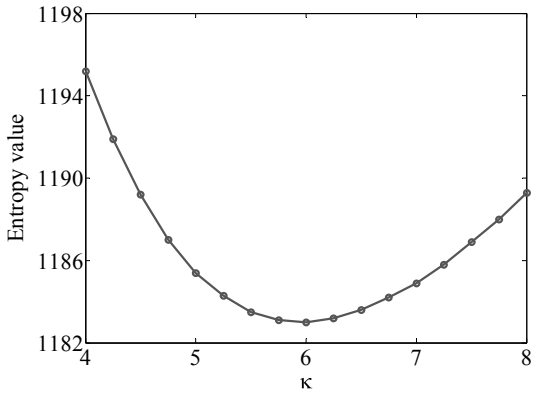


Fig. 10. Entropy value versus $\kappa$ for the time-frequency plane of the experimental signal.

detect the crack. Since wafer-type PZT sensor has the wavelength tuning effect for Lamb waves detection [21,22], i.e. for a given length PZT sensor, the sensed wave signal has very large amplitude when the wavelength is about twice the length of PZT sensor. A very short PZT sensor is calibrated in the experiment, so that the signal of the large amplitude, high frequency component $A_0$ Lamb waves can be detected. An impact hammer is used as excitation source; the impact position is same with the bonding position of PZT sensor 1, but is onto the opposite surface of the beam. The data is acquired using an oscilloscope (Yokogawa DL1540C). The location of the PZT sensors and crack and the span of the beam are illustrated in Fig. 8. Note that the crack is introduced into the beam after the estimation of the GVDC.

When the hammer impacts the beam surface in a very short time, the sensing voltage from sensor 1 exceeds the threshold value almost simultaneously. The digital oscilloscope will begin to record the whole time response data from sensor 1. The sampling frequency for each channel is prescribed at 1 MHz and 10018 data were captured.

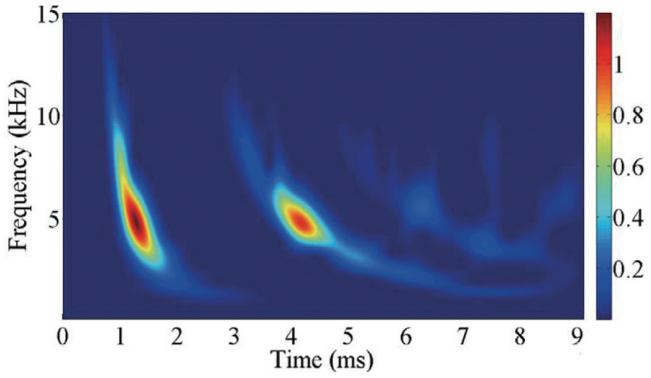


Fig. 11. Time-frequency plane with $\kappa_{opt} = 6.0$ for the pristine beam.

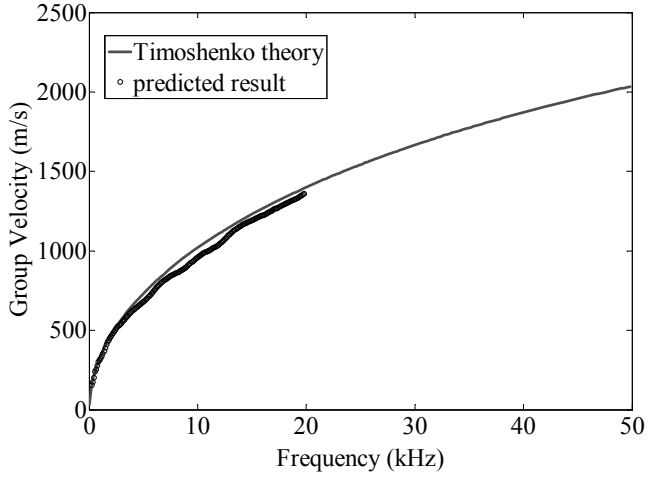


Fig. 12. GVDC of $A_0$ Lamb wave in beam estimated from experimental signal.

Figure 9 shows a typical time response signal acquired from sensor 1, which is used to estimate the GVDC of $A_0$ Lamb waves mode.

The optimal value $\kappa_{opt}$ for the signal is first calculated based on Shannon entropy function. Figure 10 shows the entropy value versus $\kappa$ in the range of 4–8, and the optimal value is $\kappa_{opt} = 6.0$. The time-frequency distribution plane with the optimal value is displayed in Fig. 11. The different value of $\kappa_{opt}$ for these two different signals obtained from the simulation and experiment demonstrates that it is a signal-dependent parameter. Subsequently the GVDC of $A_0$ Lamb waves mode is estimated from the signal and shown in Fig. 12. The result excellently agrees with the theoretical dispersion curve of Timoshenko theory.

### *4.3. Crack localization in experiment with using FSWT*

A transverse crack is introduced into the identical beam structure described above. The transverse crack in depth of 0.5 mm is cut at 700 mm on the right of the sensor 2 (refer to Fig. 8 and Fig. 13). A typical measured signal from sensor 1 for this state is shown in Fig. 14. As the hammer is operated manually, it is difficult to keep the impact force and position consistent. Therefore, it is not feasible to identify the damage by subtracting reference signal from monitored signal. In this case, the signal measured at damaged state can be only used. Due to the strongly dispersive characteristic of $A_0$ Lamb waves, it is impossible to identify the crack location from the damaged signal in the time domain. Hence, FSWT-based time-frequency analysis for the damaged signal is performed, and the resulting time-frequency plane is shown in Fig. 15. Comparing the time-frequency plane for the damaged beam with

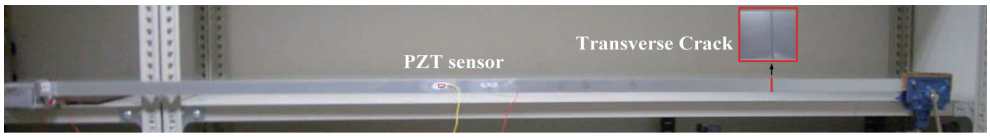


Fig. 13. Aluminum beam specimen with transverse crack.

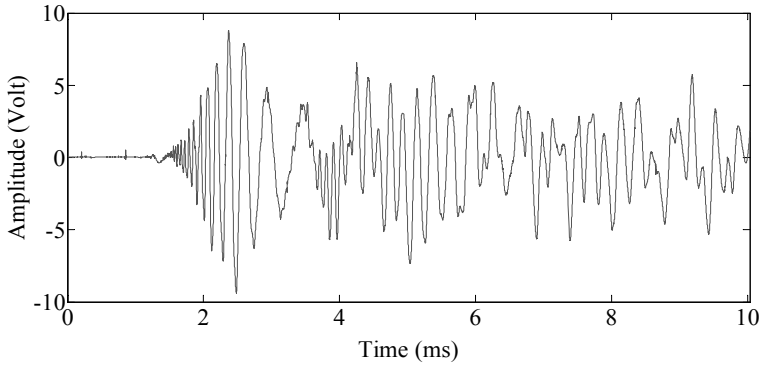


Fig. 14. Time response signal measured from sensor 2 at damaged state.

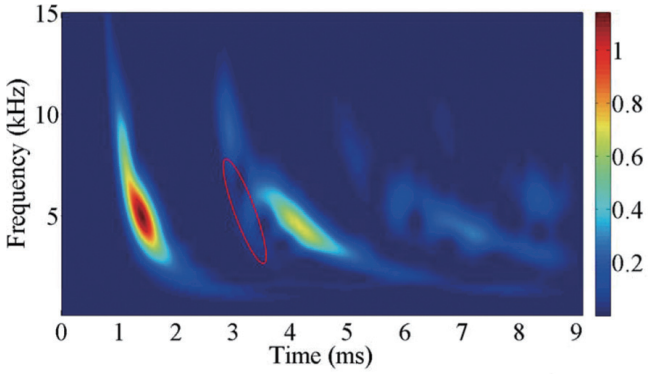


Fig. 15. Time-frequency distribution plane with $\kappa_{opt} = 6.0$ for the damaged beam.

that for the pristine beam, it is observed that in the frequency range of 3.5–7.0 kHz there is an additional local ridge marked with red ellipse.

In order to accurately identify this tiny ridge, several frequency components between 3.5–7.0 kHz are selected from the time-frequency plane and shown in Fig. 16, superposed with that for the pristine beam. For each individual frequency component, a small peak is clearly observed. The small peak indicates the arrival time of the reflection wave from the crack. Since the group velocity has been estimated, the crack location can be derived based on the length of beam, the position of the impact force and the PZT sensor. Nevertheless, the accuracy of crack localization is strongly dependent on the selection of the individual frequency component, as the interaction of Lamb waves with the crack changes with frequency. To reduce the error of damage localization from this source, three individual frequency components of 4.35, 5.09 and 6.99 kHz are used together for damage localization. Based on the arrival time of the reflection wave from the crack and the estimated group velocities, the distance of the propagation path for each individual frequency component is yielded as the product of the arrival time and group velocity. The propagation distance for these frequency components are listed in Table 1. Since the actual distance is 2242 mm, the error for each frequency component is also given in Table 1. Then the averaged distance is calculated as

Table 1
Estimated propagation distance from the crack

| Frequency (kHz) | Arrival time (ms) | Group velocity (m/s) | Total distance (mm) | Error (%) |
|---|---|---|---|---|
| $f_1 = 4.35$ | $t_{d1} = 3.170$ | $c_{g1} = 677.4$ | $d_1 = 2147.4$ | 4.2 |
| $f_2 = 5.09$ | $t_{d2} = 3.203$ | $c_{g2} = 685.0$ | $d_2 = 2194.0$ | 2.1 |
| $f_3 = 6.99$ | $t_{d3} = 2.828$ | $c_{g3} = 816.7$ | $d_3 = 2310.0$ | 3.0 |
| – | – | – | $d_{ave} = 2217.1$ | 1.12 |

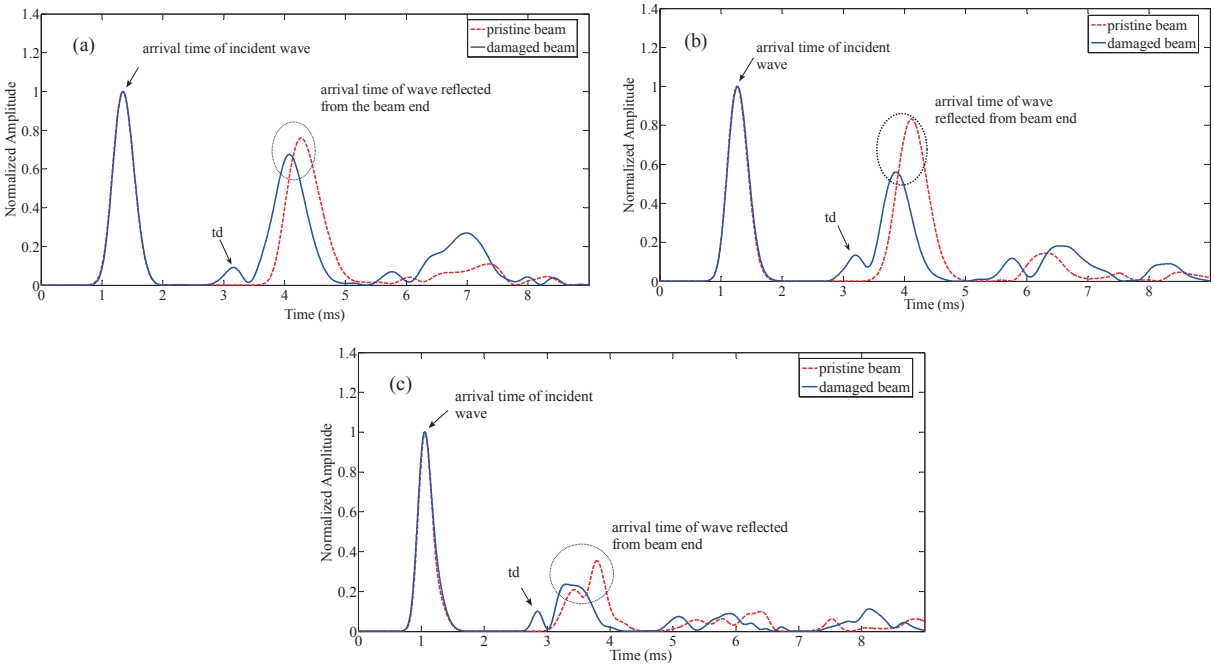


Fig. 16. Square coefficient of FSWT at (a) 4.35, (b) 5.09 and (c) 6.99 kHz in time axis.

$$d_{ave} = \frac{1}{n}\sum_{1}^{n} t_{di} c_{gi} \tag{12}$$

where $t_{di}$ and $c_{gi}$ is the arrival time and group velocity for the $i$th individual frequency component and $n$ is the number of the individual frequency component. By this operation, the error can be reduced significantly, and the result is listed in Table 1.

## 5. Conclusion

In this paper, crack localization in beam structure is conducted using impact-induced Lamb wave and FSWT-based time-frequency analysis. In order for improving the accuracy of damage localization, the optimal time-frequency resolution is achieved in the implementation of FSWT, where the parameter value $\kappa$ uniquely controlling time-frequency resolution is determined based on the proposed generalized criterion of Shannon entropy.

During the process of damage localization, the GVDC of $A_0$ Lamb waves in beam is first accurately estimated by FSWT-based time-frequency analysis. In the next, a transverse crack is introduced into the beam structure. The time response signal measured at damaged state is transformed into time-frequency plane by FSWT. From observing the variation in the time-frequency plane, the frequency range implying the presence of damage is roughly determined. To reduce the error of damage localization resulted from subjective selection of individual frequency component, several individual frequency components are selected to calculate the propagation distance of the wave reflected from crack. Then an average operation on the distance yielded from these individual frequency components is performed to improve the accuracy of damage localization.

## References


[1] D.N. Alleyne and P. Cawley, The Interaction of Lamb waves with defects, *IEEE Trans Ultrason, Ferroelectr, Freq Control* **39** (1992), 381–397.

[2] N. Hu, T. Shimomukai, H. Fukunaga and Z. Su, Damage identification of Metallic Structures Using $A_0$ mode of Lamb waves, *Struct Health Monit* **7** (2008), 271–285.

[3] P.S. Tua, S.T. Quek and Q. Wang, Detection of cracks in plates using piezo-actuated Lamb waves, *Smart Mater Struct* **13** (2004), 643–660.

[4] H. Sohn, G. Park, J.R. Wait, N.P. Limback and C.R. Farrar, Wavelet-based active sensing for delamination detection in composite structure, *Smart Mater Struct* **13** (2004), 153–160.

[5] W. Ostachowicz, P. Kudela, P. Malinowski and T. Wandowski, Damage localization in plate-like structures based on PZT sensors, *Mech Syst Signal Pr* **23** (2009), 1805–1829.

[6] K.H. Ip and Y.W. Mai, Delamination detection in smart composite beams using Lamb waves, *Smart Mater Struc* **13** (2004), 544–551.

[7] S.S. Kessler, S.M. Spearing and C. Soutis, Damage detection in composite materials using Lamb wave methods, *Smart Mater Struct* **11** (2002), 269–278.

[8] D.N. Alleyne and P. Cawley, Optimization of Lamb wave inspection techniques, *NDT & E international* **25** (1992), 11–22.

[9] P.D. Wilcox, Mode and transducer selection for long range Lamb wave inspection, *J Intel Mmater Syst Str* **12** (2001), 553–565.

[10] Y.Y. Kim and E.H. Kim, Effectiveness of the continuous wavelet transform in the analysis of some dispersive elastic waves, *J Acoust Soc Am* **110** (2001), 86–94.

[11] Z.H. Yan, A. Miyamoto and Z. W. Jiang, Frequency slice wavelet transform for transient vibration response analysis, *Mech Syst Sigal Pr* **23** (2009), 1474–1489.

[12] J.C. Hong and Y.Y. Kim, Determination of optimal Gabor wavelet shape for the best-time-frequency localization using the entropy concept, *Exp Mech* **44** (2004), 387–395.

[13] S.T. Quek, Q. Wang, L. Zhong and K.H. Ong, Practical issues in the detection of damage in beams using wavelets, *Smart Mater Struct* **10** (2001), 1009–1017.

[14] Z.H. Yan, A. Miyamoto, Z.W. Jiang and X.L. Liu, An overall theoretical description of frequency slice wavelet transform, *Mech Syst Sigal Pr* **24** (2009), 491–507.

[15] C. Shannon, A mathematical theory of communication, *Bell System Technology* **27** (1948), 379–656.

[16] Y. Lu, X. Wang, J. Tang and Y. Ding, Damage detection using piezoelectric transducers and the Lamb wave approach?: Robust and quantitative decision making, *Smart Mater Struct* **17** (2008), 1–13.

[17] D.C. Worlton, Experimental confirmation of Lamb waves at megacycle frequencies, *Journal of Applied Physics* **32** (1961), 967–971.

[18] K.F. Graff, Wave Motion in Solids, *Dover*, New York, 1975, 155–186.

[19] A. Liang, *Asymptotic Wave Solutions for Euler-Bernoulli and Timoshenko Beam by Ray Method and Stationary Phase Method*, Master Thesis, North Carolina State University, 2003.

[20] ANSYS 2005, Theory Reference for ANSYS: Release 10.0 (Canonsburg, PA: ANSYS Inc.)

[21] W.J. Staszewski, B.C. Lee, L. Mallet and F. Scarpa, Structural health monitoring using scanning laser vibrometry: Lamb wave sensing, *Smart Mater Struct* **13** (2004), 251–260.

[22] V. Giurgiutiu, Tuned Lamb wave excitation and detection with piezoelectric wafer active sensors for structural health monitoring, *Journal of Intelligent Material Systems and Structures* **16** (2005), 291–305.